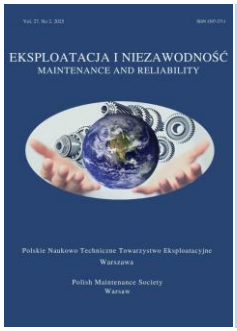

Eksploatacja i Niezawodnosc – Maintenance and Reliability
Volume 27 (2025), Issue 2
journal homepage: http://www.ein.org.pl

Article citation info:
Lao J, Wang X, Zhang M, Chen Z, Guo J, Analysis and Improvement of Coal-loading Performance and Reliability of Thin Seam Coal Shearer Drums, Eksploatacja i Niezawodnosc – Maintenance and Reliability 2025: 27(2) http://doi.org/10.17531/ein/194674

Analysis and Improvement of Coal-loading Performance and Reliability of Thin Seam Coal Shearer Drums

Indexed by: Web of Science Group

Junming Lao[a], Xuecheng Wang[b,*], Mengqi Zhang[c], Zhi Chen[a], Jianfeng Guo[a]

[a] Taiyuan University of Science and Technology, China
[b] Shanxi Tiandi Coal Machinery Co.Ltd, China
[c] Shanxi Institute of Energy, China

Highlights

- A collaborative optimization method based on an improved NSGA-II algorithm is proposed.
- Two types of coal-guiding drums are designed and analyzed.
- An improved NSGA-II strategy based on spatial density is introduced.
- This collaborative optimization method significantly enhances the reliability of the drum.

Abstract

The structure of coal shearer drums significantly influences the coal-loading efficiency and load fluctuations of thin seam coal shearers. To enhance drum efficiency and reliability, this paper proposes a collaborative optimization method based on an improved NSGA-II algorithm. Initially, using the Discrete Element Method (DEM), we analyze the impact of helical vanes on coal-loading performance and investigate novel designs for two types of coal-guiding drums. To optimize dynamic performance, concepts like spatial density and adaptive radius are introduced, proposing an NSGA-II enhancement strategy based on spatial density for the collaborative optimization of drum structure and motion parameters. Finally, the entropy-weighted TOPSIS method is used for subjective evaluation to select the optimal solution. Research findings demonstrate that this collaborative optimization method significantly enhances drum reliability, reduces load fluctuations by 46.34%, increases coal-loading efficiency by 7.06%, and decreases coal-loading power by 27.31%.

Keywords
thin seam coal mining machines, coal-loading performance, reliability; NSGA-II, collaborative optimization

1. Introduction

Coal is one of the most abundant fossil fuels on Earth, accounting for 30% of primary energy sources [1]. There are vast reserves of thin coal seams globally, and with advancements in technology and increasing market demand, the mining of thin coal seams has become an economically viable option. Due to the thickness of thin coal seams not exceeding 1.5 meters, the diameter of the mining machine drum is limited by the working space, which affects the overall performance of the drum [2, 3].

In the actual coal-loading process, coal particles often experience blockage, significantly reducing the drum's coal-loading performance [4]. In order to enhance the coal-loading performance of coal miner drums, scholars have studied the structural and kinematic parameters of the drums and analyzed the potential impact of these factors on the coal-loading performance. Sun compared the coal-loading performance of

(*) Corresponding author.
E-mail addresses: J. Lao (ORCID: 0009-0003-7355-8283) s202212110034@stu.tyust.edu.cn, X. Wang wxc_zmk@126.com, M. Zhang (ORCID: 0000-0001-9567-4240) dreamci@163.com, Z. Chen mechenzhi@tyust.edu.cn, J. Guo s202312210071@ stu.tyust.edu.cn

coal mining machine drums and spiral conveyors, studying the effect of blade axial inclination angle on the coal-loading performance of the drum, and established the relationship between the coal-loading performance of coal mining machine drums and factors such as vane axial inclination angle, style, hub shape, and diameter [5]. Zhang studied two coal discharge methods, namely projection and extrusion, and obtained the law of the effect of drum diameter on the axial velocity, coal-loading velocity, and trough depth of coal particles [6].

Conventional thin seam coal miner drums usually use relatively simple helical vanes. In the coal cutting stage, the picks are in contact with the coal wall and are subject to large loads, which are easy to wear out, but it is more convenient to replace the picks after wear. However, in the coal loading stage, the vanes are subjected to impact loads and wear severely, resulting in a significant decrease in the drum's coal-loading performance after its failure, and it is also more troublesome to replace and repair the vanes, which significantly reduces the overall production efficiency [7]. Wan, through the analysis of the dynamic response of cutting equipment, discovered that impact loads are the primary cause of drum vibration [8]. Meng proposed a mechanical-hydraulic co-simulation method to study the dynamic response of Chock-shield supports to impact loads. The research results indicate that this method can accurately identify the dangerous points of hydraulic support reliability[9]. Zhang designed a multi-point impact drum, and through discrete element coal breaking experiments, it was found that the multi-point impact drum could improve its performance by more than 20% in terms of both coal breaking capacity and reduction of unit energy consumption [10]. Gao proposed a double-stage differential rotation drum, and the study showed that the drum's coal-loading performance was optimized when the helix angle of the front drum was 18° and the helix angle of the rear drum was 30° [11].

Discrete Element Method (DEM) is currently a primary method used to address particle-related issues, where it simulates the movement of materials using particles, with particle motion and force complying with Newton's laws. P.A. Cundall first applied DEM to studies related to rock structures [12]. Liu analyzed the wear of mining machine vanes using EDEM discrete element simulation software, obtaining the wear patterns of the helical vanes [13].

On the other hand, multi-objective intelligent algorithms are increasingly applied in engineering to solve optimization problems with multiple interrelated objectives. Currently, there are many intelligent optimization algorithms and improvement strategies[14-16]. NSGA-II is one of the most mainstream multi-objective genetic algorithms, with advantages mainly in non-dominated sorting, diversity preservation, and strong adaptability [17-21]. When a problem has multiple interrelated objectives, NSGA-II can provide better performance and a more comprehensive solution set [22-26]. Liu established a multi-objective optimization function with traction speed as the design variable and drum load, reduced specific energy consumption, and coal loading rate as comprehensive indicators. They used the NSGA-II optimization algorithm to obtain the optimal traction speed and experimentally validated the accuracy of the simulation[27]. Hao introduced adaptive balance parameters to improve the convergence and solution set diversity of the NSGA-II algorithm, and through benchmark test functions and practical applications, demonstrated the superior characteristics of the improved NSGA-II algorithm [28]. Chen validated the reliability of DEM simulations and obtained the optimal design parameters for the screw conveyor using the NSGA-II multi-objective optimization algorithm[29].

Past studies have mainly analyzed the performance of screw drums through theoretical, experimental, numerical analysis, and intelligent algorithms, achieving significant results [30-33]. However, these studies mainly focused on the existing structure of the drum, using single-factor control methods to investigate the effect of mining machine operating parameters on drum performance [34-37]. In terms of drum design, the research on drum performance is more insufficient. In this paper, the helical vane of the drum is taken as the research object from the design point of view. The influence of parameters such as helical angle, axial velocity of coal particles and mass flow rate on dynamic coal-loading performance is systematically studied. The structure of the drum is optimized, and the difference in coal-loading performance and reliability with the traditional drum is analyzed qualitatively and quantitatively. Finally, the improved NSGA-II algorithm was used to co-optimize the drum to further improve the performance of the screw drum.

2. Methods and Models

2.1. Collaborative Optimization Method

To address the issues of low coal-loading efficiency and large load fluctuations in traditional shearer drums during coal particle coal loading, this paper proposes a collaborative optimization method, as illustrated in Figure 1. First, the helical angle that maximizes coal-loading efficiency is determined. Then, based on this optimal helical angle, two types of coal-guiding drums are designed. To further optimize the performance of the drums, the improved NSGA-II algorithm is utilized for the collaborative optimization of the drums' motion parameters. Finally, the optimized scheme is compared with the pre-optimized drums to evaluate the performance improvement. This systematic optimization method can significantly enhance the coal-loading efficiency of the drums and reduce load fluctuations.

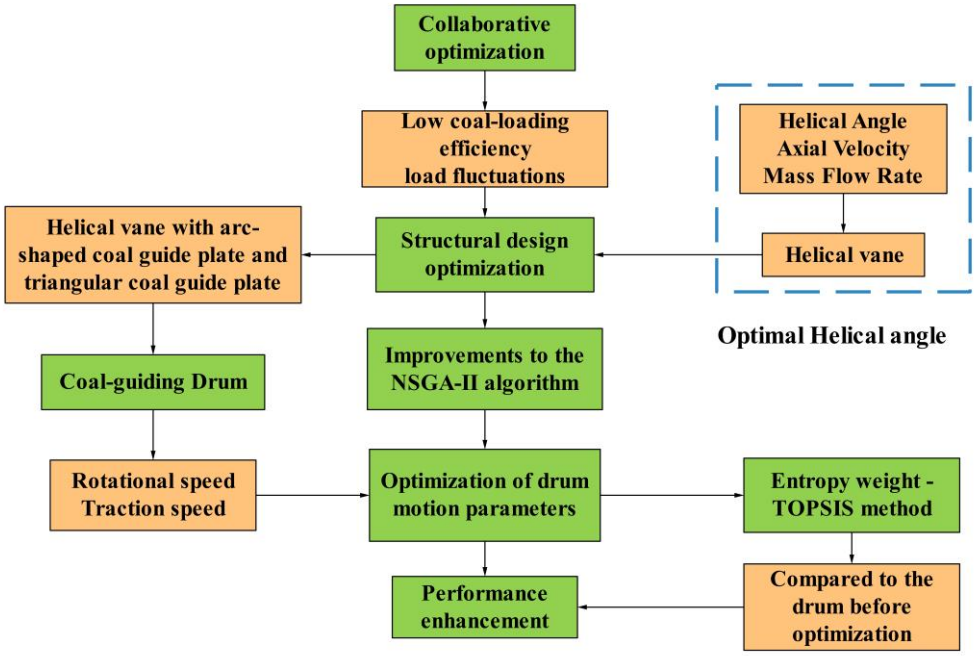

Figure 1. Flowchart of the Collaborative Optimization Method.

2.2. Establishment of the Discrete Element Model

2.2.1. Selection of the Contact Model

The Discrete Element Method primarily simulates the contact forces between particles by computing their forces and displacement relationships, deriving particle displacement and velocity information based on Newton's second law. The cutting and coal-loading process of coal-rock can be regarded as the fragmentation and transportation of the entire mass composed of a series of discrete coal particles under the action of the screw drum. To enhance computational accuracy, this study employs the Hertz-Mindlin (no-slip) contact model as the theoretical foundation, where the relationship between the forces and displacements among particles is expressed as Equation (1).

$$\begin{cases} F_n = \frac{4}{3} E^* (R^*)^{\frac{1}{2}} \delta_n^{\frac{3}{2}} \\ F_t = -S_t \delta_t \end{cases} \quad (1)$$

In the equations: F_n represents the normal force, N; E^* represents the equivalent Young's modulus, Pa; R^* represents the equivalent radius, m; δ_n represents the normal overlap, m; F_t represents the tangential force, N; S_t represents the tangential stiffness, N/m; and δ_t represents the tangential overlap, m.

Before the drum cuts the coal-rock, the Bonding-Particle model is chosen to simulate the stability of the particles, which generates adhesive forces within a certain radius range to bind the particles together. When the force on the particle reaches the maximum normal and tangential shear, the band bond breaks and the contact model changes from the Bonding-Particle model to the Hertz-Mindlin model, as shown in Figure 2.

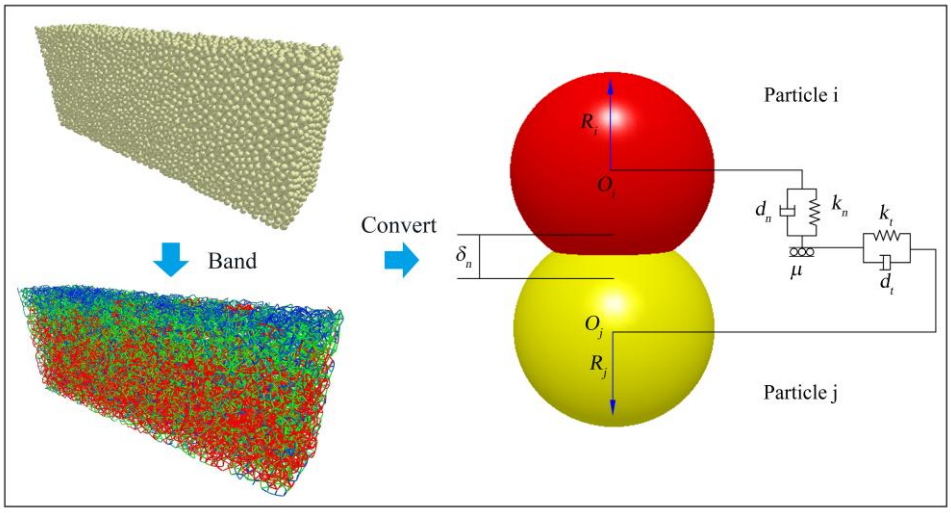

Figure 2. Discrete Element Model.

2.2.2. Setting of Particle Parameters

Based on the widespread application of bituminous coal in coal mining engineering and its complex physical properties, this study adopts bituminous coal sampled from a coal mine in Ordos City, Inner Mongolia, China, as the experimental object [38], with relevant parameters shown in Table 1 below.

Table 1. Coal Particle Parameters Table.

Tensile strength (MPa)	Compressive strength (MPa)	Modulus of elasticity (MPa)	Poisson's ratioμ	Cohesive force (MPa)	Angle of internal friction (°)	Coefficient of robustness f
1.08	17.71	4388	0.23	1.85	59	2

The setting of Bonding has an important influence on the simulation of drum cutting, so the stiffness coefficient of Bonding is calculated as follows. According to the Mohr-Coulomb strength theory, the shear stress on the coal-rock fracture surface is the sum of its cohesion and the friction force generated by the normal stress on the fracture surface, as shown in Equation (2).

$$\begin{cases} \sigma = \frac{1}{2}(\alpha_1 + \alpha_3) + \frac{1}{2}(\alpha_1 - \alpha_3)\cos 2\alpha \\ \tau = \frac{1}{2}(\alpha_1 - \alpha_3)\sin 2\alpha \\ \alpha = \frac{\pi}{4} + \frac{\varphi}{2} \end{cases} \quad (2)$$

$$\tau = C + \sigma \tan\varphi \quad (3)$$

In this equation: σ is the axial compressive strength, MPa; α_1 is the maximum principal stress, MPa; α_3 is the minimum principal stress, MPa;$\tau$is the damage surface shear stress, MPa; $\alpha$is the damage angle, °;$\varphi$the internal friction angle, °;$C$is the cohesive force, MPa

According to the modified Griffith's formula

$$\begin{cases} \sigma_1 = -\frac{4\sigma_t}{(1-\frac{\sigma_3}{\sigma_1})\sqrt{1+\mu^2}-\mu(1+\frac{\sigma_3}{\sigma_1})} \\ \frac{\sigma_1}{\sigma_c} = \frac{\sigma_3}{\sigma_c} \times \frac{\sqrt{1+\mu^2}+\mu}{\sqrt{1+\mu^2}-\mu} + 1 \end{cases} \quad (4)$$

In this equation:$\sigma_t$is the tensile strength of the material, MPa;$\mu$is the friction coefficient between the cracks;$\sigma_c$is the compressive strength of the material, MPa

The stiffness coefficient is calculated using the formula

$$\begin{cases} k_n = \frac{4}{3}\left(\frac{1-v_1^2}{E_1} + \frac{1-v_2^2}{E_2}\right)^{-1}\left(\frac{r_1+r_2}{r_1 r_2}\right)^{-1/2} \\ k_s = (1/2 \sim 2/3)k_n \end{cases} \quad (5)$$

In this equation: k_n is the normal stiffness coefficient, N/m; v_1 and v_2 are the Poisson's ratio of the two particles; E_1 and E_2 are the modulus of elasticity of the two particles, Pa;$r_1$and$r_2$are the radius of the two particles, m;$k_s$is the tangential stiffness.

In the simulation experiments, the size and shape of coal particles significantly affect the simulation accuracy and computational efficiency. To accurately simulate the crushing and transportation process of coal, this study selected spherical particles with a diameter of 25 mm. The normal and tangential stresses on the rupture surface were calculated using the Mohr strength theory formula (2), and the normal and tangential stiffness coefficients were calculated using formulas (4) and (5). The calculation results are shown in Table 2.

Table 2. Coal block contact parameters.

Component	Value
Normal stress/MPa	7.7e+09
Tangential stress/MPa	4.47e+09
Normal stiffness factor/（N/m）	2.615e+06
Tangential stiffness factor/（N/m）	1.76e+06

2.2.3. Establishment of the Drum

The helical angle of vanes is a key design parameter affecting the coal-loading performance of the shearer drum, and its proper setting has a significant impact on improving the coal-loading effect of the drum. Four different drums with different helical angles were used in the test, and the rest of the structural parameters were the same, as shown in Figure 3 below. The specific parameters are shown in Table 3 below.

Table 3. Drum specific parameters.

Component	Value
helical angles	12°、18°、24°、30°
Cylinder diameter (mm)	700
Vanes diameter (mm)	1200
Cylinder width (mm)	700
Screw number	3

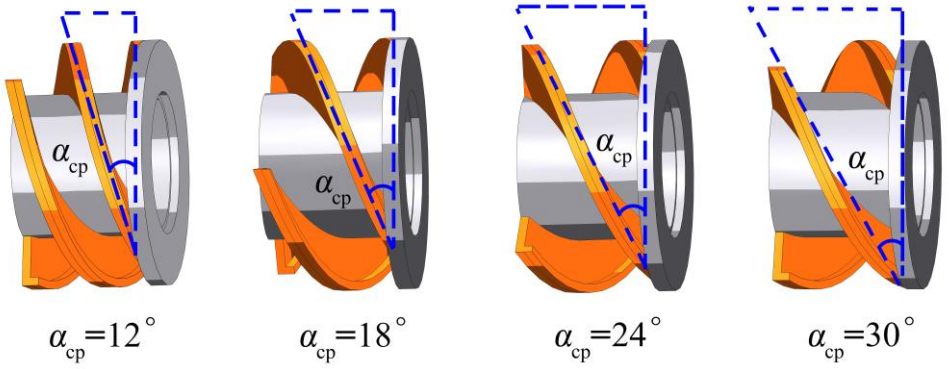

Figure 3. Drums with Different helical Angles.

This paper designs two kinds of coal-guiding drums with a helical angle of 18°. That is, a circular arc-shaped coal guide plate is added at the root of the helical vanes of the traditional drum, which is labeled as Structure 1#; a triangular coal guide plate continues to be added at the tail end of the Structure 1# drum, which is labeled as Structure 2#, as shown in Figure 4 below. The specific parameters of the drum are shown in Table 4. This design aims to significantly improve the coal-loading efficiency of the coal miner and reduce the load fluctuation during the coal-loading process in order to enhance the overall performance and working efficiency.

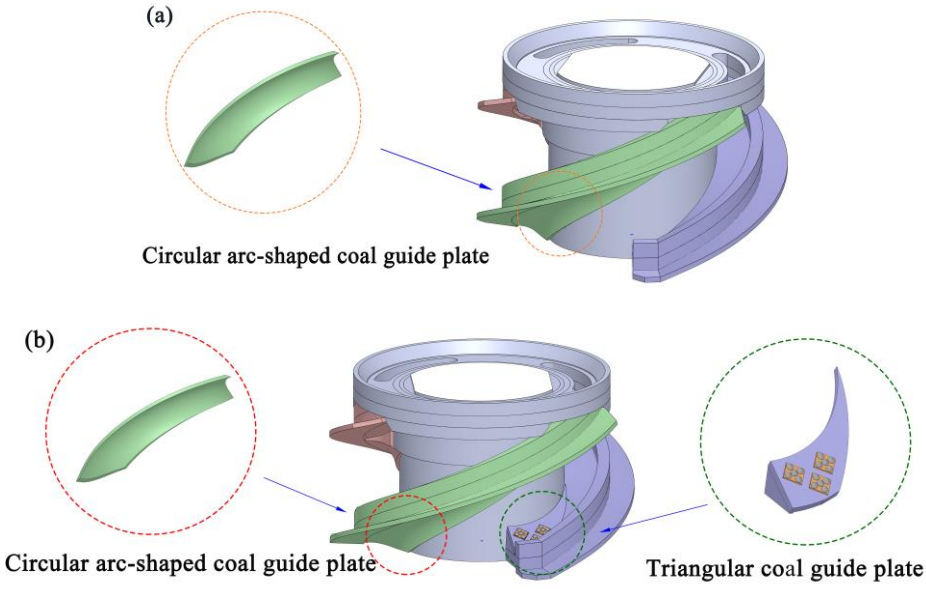

Figure 4. Structure of the Coal-guiding Drum (a) Structure 1# (b) Structure 2#.

Table 4. Specific Parameters of the Drum.

Component	Value	Component	Value
Structure 1#		Structure 2#	
Cylinder diameter (mm)	700	Cylinder diameter (mm)	700
Vanes diameter (mm)	1200	Vanes diameter (mm)	1200
Cylinder width (mm)	720	Cylinder width (mm)	720
Helical angle (°)	18	Helical angle (°)	18
Screw number	3	Screw number	3
Number of circular arc-shaped coal guide plates	3	Number of circular arc-shaped coal guide plates	3
Number of triangular coal guide plates	0	Number of triangular coal guide plates	3

2.3. Establishment of the Motion Model

The loading of coal particles primarily relies on the rotation of the coal mining machine drum, which forms a coal flow through the action of the helical vanes, with the velocity of the coal flow ranging between the minimum and maximum coal particle velocities. To understand the motion characteristics of the coal flow during the operation of the drum, individual coal particles are taken as the research object, and their motion is analyzed, as shown in Figure 5. It is assumed that there is no relative motion between the coal particles, and the velocity of the coal flow is equal to the velocity of the coal particles.

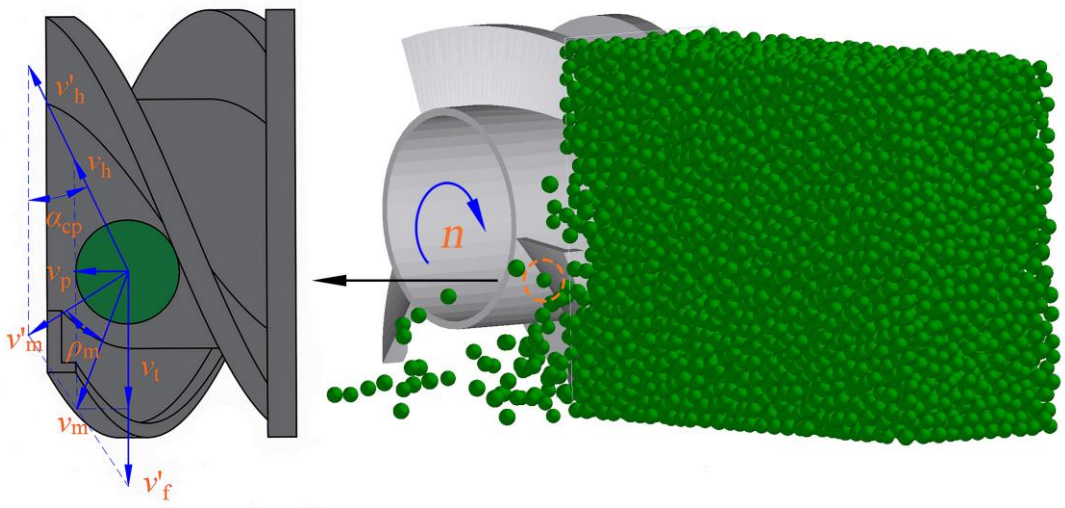

Figure 5. Motion Analysis of Individual Coal Particles.

During the drum cutting process, the gravitational force acting on the coal chunks is relatively small compared to the compressive force. Therefore, in the velocity analysis, the weight of the coal chunks is neglected. The coal chunks move with an absolute velocity $v'_m = v'_f + v'_h$, but due to the friction between the coal chunks and the helical vanes, a friction angle is generated, causing the absolute velocity to become $v_m = v'_f = v_h$.

According to the velocity projection theorem, the absolute velocity of the coal chunk after the action of friction force:

$$vm = nL_{\text{cp}} \frac{cos\ \alpha_{\text{cp}}}{cos\ \rho_m} \quad (6)$$

The pitch of the helical vanes:

$$L_{\text{cp}} = \pi D_{\text{cp}}\ tan\ \alpha\ \text{cp}$$

In the equation: v'_m represents the absolute velocity before the action of friction force, mm/s; v'_f represents the traction speed, mm/s; v'_h represents the relative velocity before the action of friction force, mm/s; ρ_m represents the friction angle between the coal chunk and the helical vane, rad; v_h represents the relative velocity after the action of friction force, mm/s; n represents the rotation speed of the drum, r/min; α_{cp} represents the helix angle of the helical vane, (°); D_{cp} represents the revolving diameter of the coal chunk on the vane, mm.

The absolute velocity v_m is projected along the axial and tangential directions to obtain the axial velocity of the coal chunk:

$$v_p = \frac{\pi n D_{\text{cp}}\ sin(\alpha_{\text{cp}}+\rho_m)}{cos\ \rho_m} \quad (7)$$

The tangential velocity of the coal chunk:

$$v_t = \frac{\pi n D_{\text{cp}}\ sin\ \alpha_{\text{cp}}\ cos(\alpha_{\text{cp}}+\rho_m)}{cos\ \rho_m} \quad (8)$$

From the formulas for the axial and tangential velocities of the coal chunk, it is evident that the axial velocity v_p and the tangential velocity v_t are positively correlated with the rotation speed and the helix angle of the spiral blade.

3. Results and Discussion

3.1. Study of the Optimum Helical Angle

The axial velocity and mass flow rate of the coal stream serve as important indicators of the coal-loading performance of the drum, crucial for assessing the coal-loading performance of the shearer. In order to further study the mining effect of the shearer drum, the quality of coal particles discharged to the scraper conveyor, that is, the ratio of the total mass of coal block in the statistical area to the total mass of coal wall cut by the drum, is taken as the evaluation index of the drum coal-loading performance, and is defined as the coal-loading efficiency, as shown in Figure 6. Additionally, three-directional forces are set for the drum, where the X-direction primarily represents resistance from the forward direction of the drum, the Y-direction denotes resistance from the measuring direction of the drum, and the Z-direction represents resistance from the bottom surface.

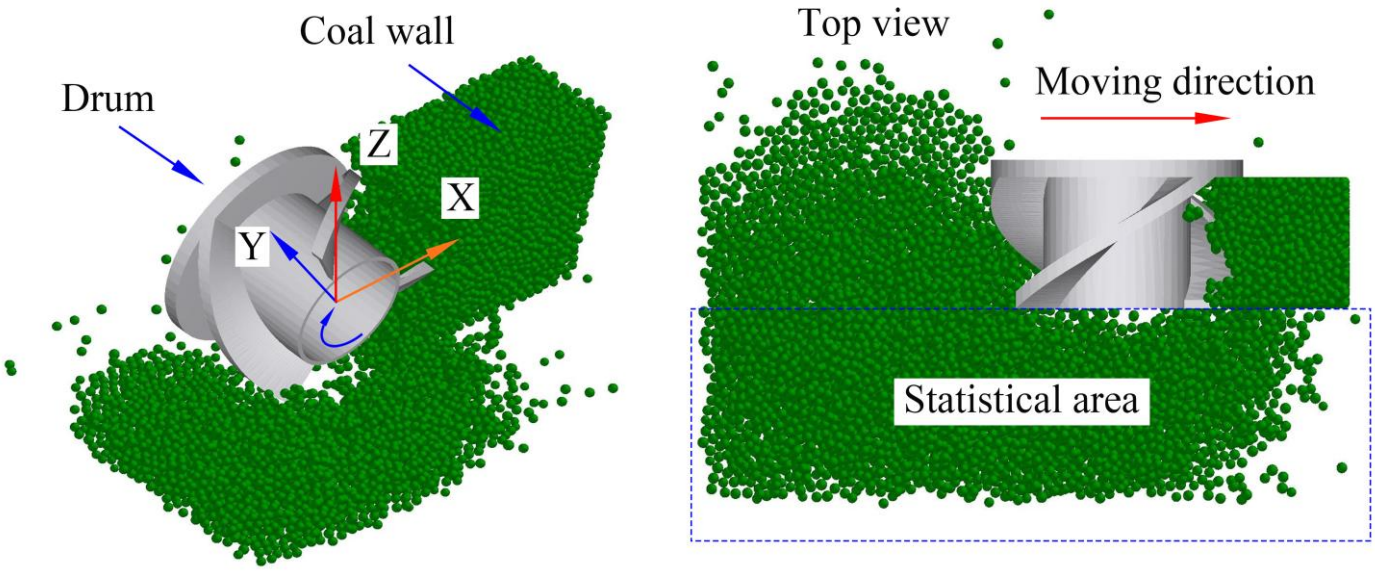

Figure 6. Coal Falling Zones.

Under conditions where the rotational speed is 58.9 r/min, and traction speeds are 50, 60, 70, 80, 90, and 100 mm/s, the coal-loading efficiency of four different helical angle drums is depicted in Figure 7.

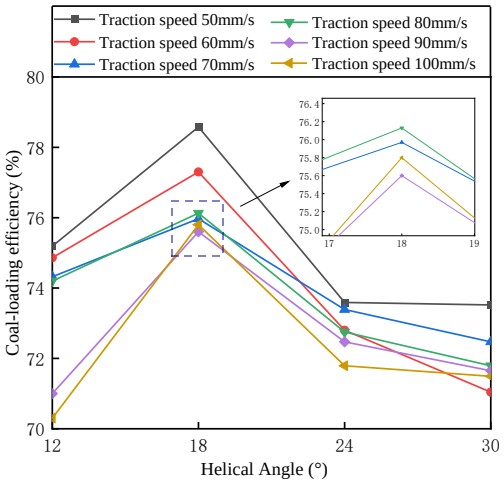

Figure 7. Influence of Helical Angle on coal-loading Efficiency.

At the same helical angle, as the traction speed increases, coal blocks tend to become unstable, jump, and break, preventing them from effectively falling into the gaps between the helical vanes and being discharged efficiently with the rotation of the drum, thereby affecting the coal-loading efficiency of the drum. This phenomenon leads to a decrease in coal-loading efficiency with increasing traction speed.

Additionally, when the helical angle is less than 18°, the coal-loading efficiency increases with the increase of the helical angle until it reaches the optimal coal-loading efficiency at 18°. However, when the helical angle exceeds 18°, the coal-loading efficiency decreases with the increase of the helical angle.

Under the condition of a rotational speed of 58.9 r/min and a traction speed of 90 mm/s, the comparison of coal-loading efficiency, axial velocity, and mass flow rate for four different helical angle drums is shown in Figure 8.

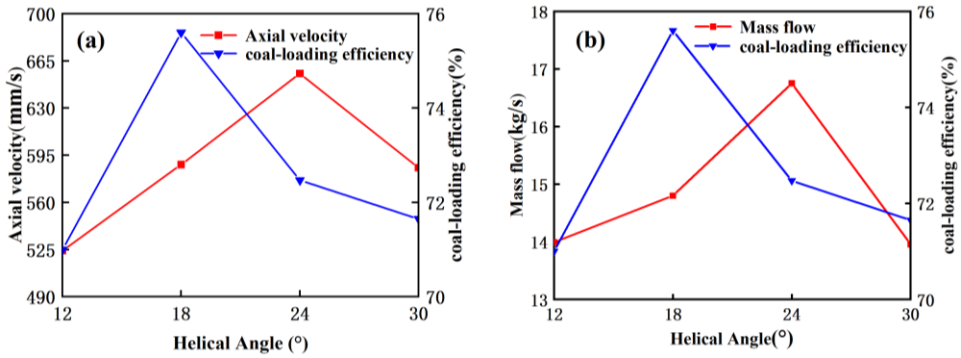

Figure 8. Relationship between Coal-loading Efficiency and Mass Flow Rate and Axial Velocity (a) Axial Velocity and Coal-loading Efficiency (b) Mass Flow Rate and Coal-loading Efficiency.

With the continuous increase of the helical angle, the cutting efficiency of the drum improves, and the axial velocity and mass flow rate of the coal flow also increase, resulting in an increase in coal-loading efficiency. However, when the helical angle exceeds a certain optimal value, the spacing between the helical lines increases, accommodating more coal blocks, which prevents effective discharge of coal particles, leading to a decrease in the axial velocity and mass flow rate of the coal flow, and consequently reducing the coal-loading efficiency of the drum.

It can be concluded that as the helical angle increases, the coal-loading efficiency of the drum gradually increases from 73.31% to 76.56%. The optimal coal-loading efficiency is achieved when the helical angle reaches 18°. As the helical angle continues to increase from 18° to 30°, the coal-loading efficiency of the drum shows a negative correlation trend with the helical angle.

3.2. Optimization Study of Vane Structure

In the drum loading process, the design of the vane structure plays a key role in the coal flow guidance and coal-loading performance. The traditional vane design suffers from low coal-loading efficiency and large load fluctuation, which affects the overall coal-loading performance. To solve these problems, the shape of the vane is optimized in this paper to better guide the coal flow and reduce the fluctuation, thus enhancing the coal-loading performance. In this section, we will deeply analyze the mechanism of the vane's influence on coal loading efficiency, analyze the performance of the optimized design in the change of the direction of the coal flow velocity, and further explore the optimized load fluctuation and its improvement effect on the drum performance.

3.2.1. Analysis of the Effect of Vane on Coal-loading Efficiency

In traditional drum designs, coal particles initially cut are influenced by gravity, falling downward along the helical vanes and subsequently discharged as the helical vanes rotate. To demonstrate the effectiveness of the optimized drum, a comparison of the velocity direction of the coal flow in the drum at different times is depicted in Figure 9.

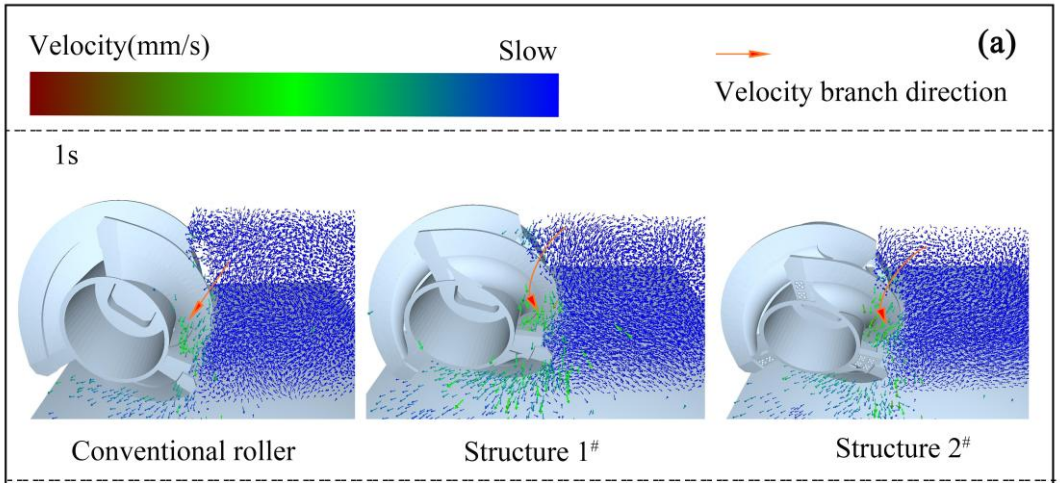

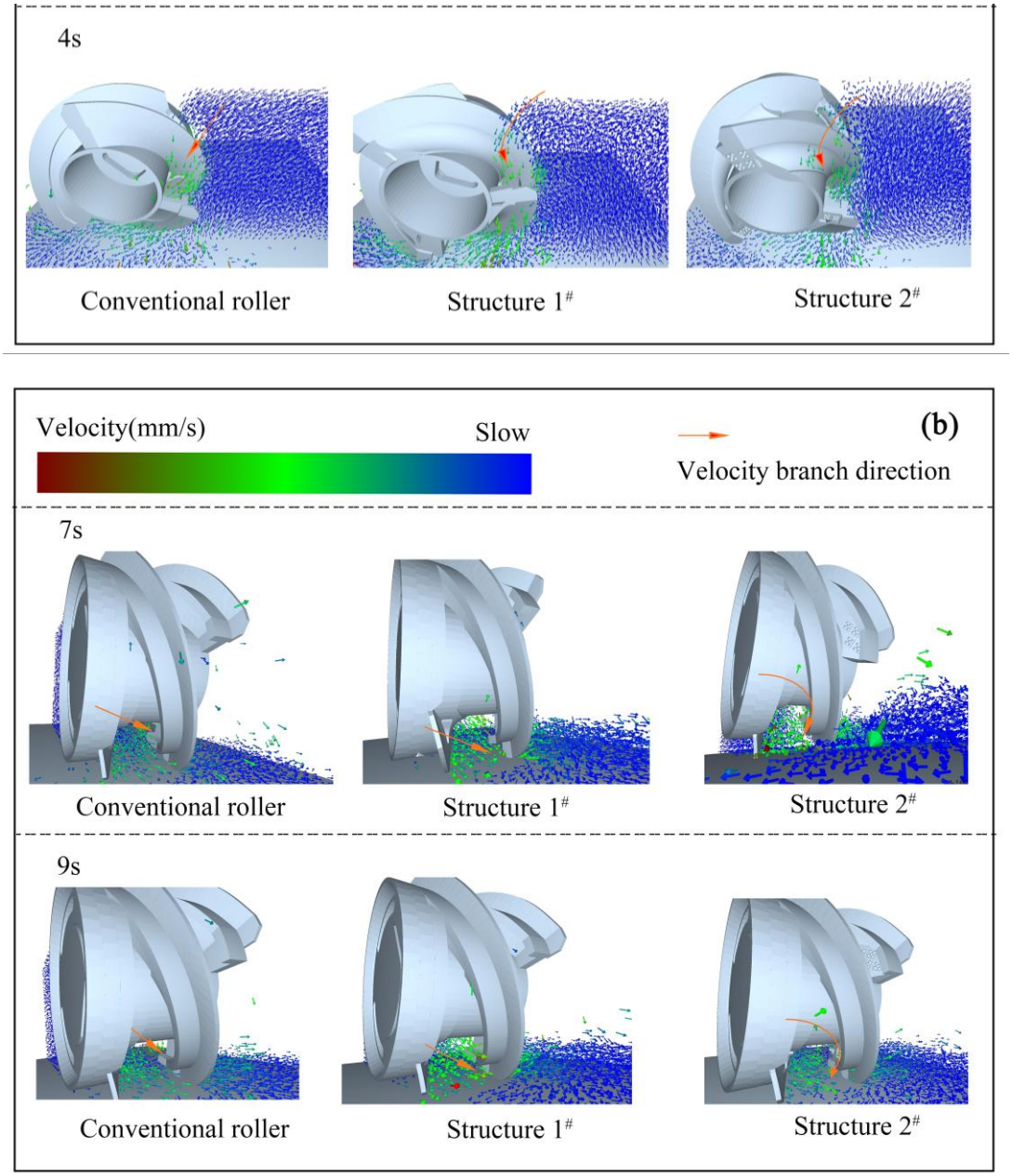

Figure 9. Effectiveness of Coal-guiding Plates (a) Comparative Effectiveness of circular arc-shaped coal guide plates (b) Comparative Effectiveness of Triangular Coal-guiding Plates.

As shown in Figure 9(a), the coal particles being cut experience an outward force from the arc-shaped coal guiding plate during the falling process, altering their trajectory and increasing their axial velocity. This makes them easier to discharge, thereby enhancing the coal-loading efficiency. As depicted in Figure 9(b), during the discharge process by the helical vanes, some coal particles may enter the inner side of adjacent helical vanes and, with the rotation of the helical vanes, be thrown to the rear of the drum, forming floating coal. By designing triangular coal guiding plates, the direction of coal flow can be adjusted, altering the velocity direction of some coal particles and thereby improving the coal-loading performance of the drum.

To more intuitively demonstrate the coal-loading performance of the optimized drum, within the range of conventional operating parameters of the drum, three rotational speeds (43.3, 50.4, and 58.9 r/min) and three traction speeds (50, 110, and 180 mm/s) were selected to study the coal-loading efficiency of the optimized coal mining machine, as shown in Figure 10.

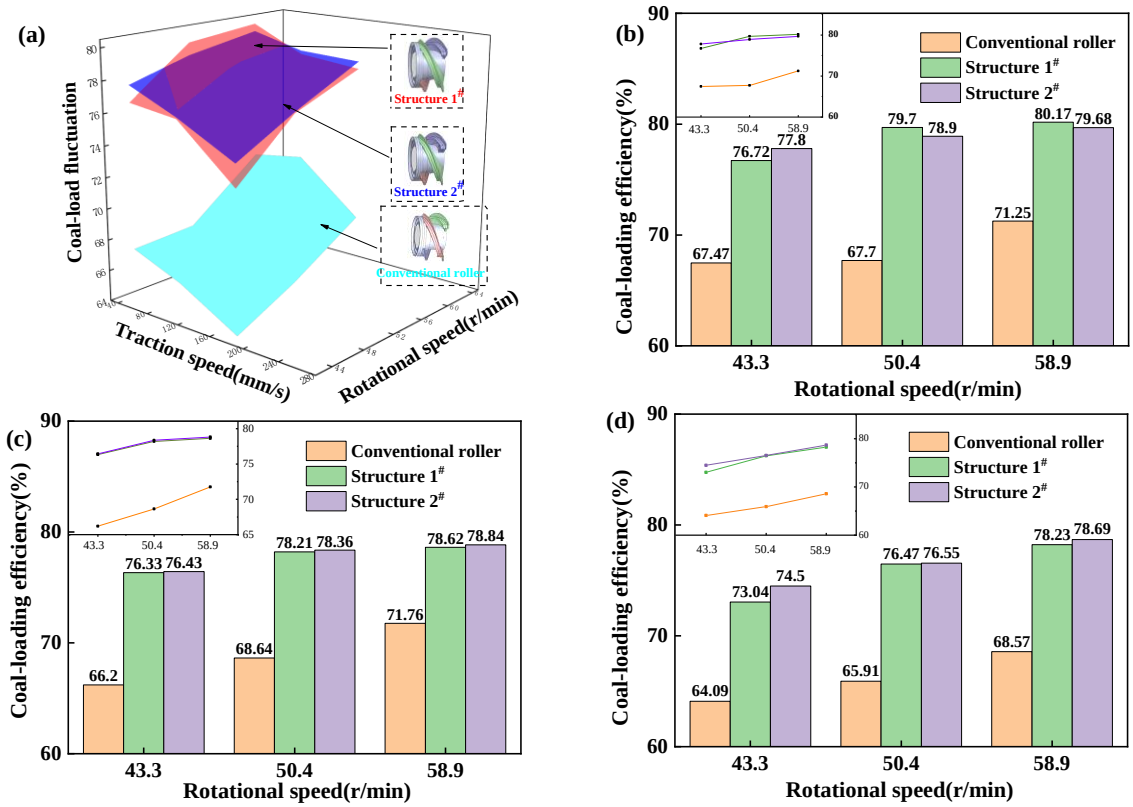

Figure 10. Coal-loading Effectiveness of Rollers Before and After Optimization (a) Coal-loading Efficiency Surface Plot (b) Traction Speed at 50 mm/s (c) Traction Speed at 110 mm/s (d) Traction Speed at 180 mm/s.

The coal-loading efficiency of Structure 1# increased by an average of 9.54%, while that of Structure 2# increased by an average of 9.80%, indicating a significant improvement in the coal-loading performance of the optimized structures. After adding the arc-shaped coal guiding plate, as the traction speed increases, more coal particles are cut but cannot be promptly and effectively discharged. Consequently, the loading efficiency decreases with increasing traction speed.

When the traction speed exceeds 110 mm/s, there are more coal particles in adjacent helical vanes. By further adding triangular coal guiding plates, some coal particles can be prevented from being thrown to the rear of the drum with the helical vanes, thereby enhancing the coal-loading efficiency of the drum. Therefore, when the traction speed exceeds 110 mm/s, the loading efficiency of Structure 2# is higher than that of Structure 1#.

3.2.2. Analysis of the Effect of Vane on Load Fluctuation

The shape of the helical vane is one of the key factors influencing the load fluctuation of the coal mining machine drum. By optimizing the structure of the s helical vane, the load fluctuation of the drum can be effectively improved. To quantitatively describe the load fluctuation of the drum, the load fluctuation coefficient is introduced:

$$\delta = \frac{1}{\overline{F}}\sqrt{\frac{\sum_{t=1}^{r}(F_t-\overline{F})^2}{r}} \tag{9}$$

The average value of the drum load:

$$\overline{F} = \frac{1}{r}\sum_{ti=1}^{r} F_{t_i}$$

In the equation: tirepresents the cutting time point of the drum, s; $r$represents the cutting end time point of the drum, s; F_t represents the instantaneous load of the drum at the corresponding time point, N.

Under the operating conditions of a traction speed of 180 mm/s and a rotation speed of 43.3 r/min, simulation experiments were conducted to study the load fluctuation of the optimized drum. The three-directional forces of the drum, as well as the average value and coefficient of fluctuation of the resultant force, are shown in Figure 11.

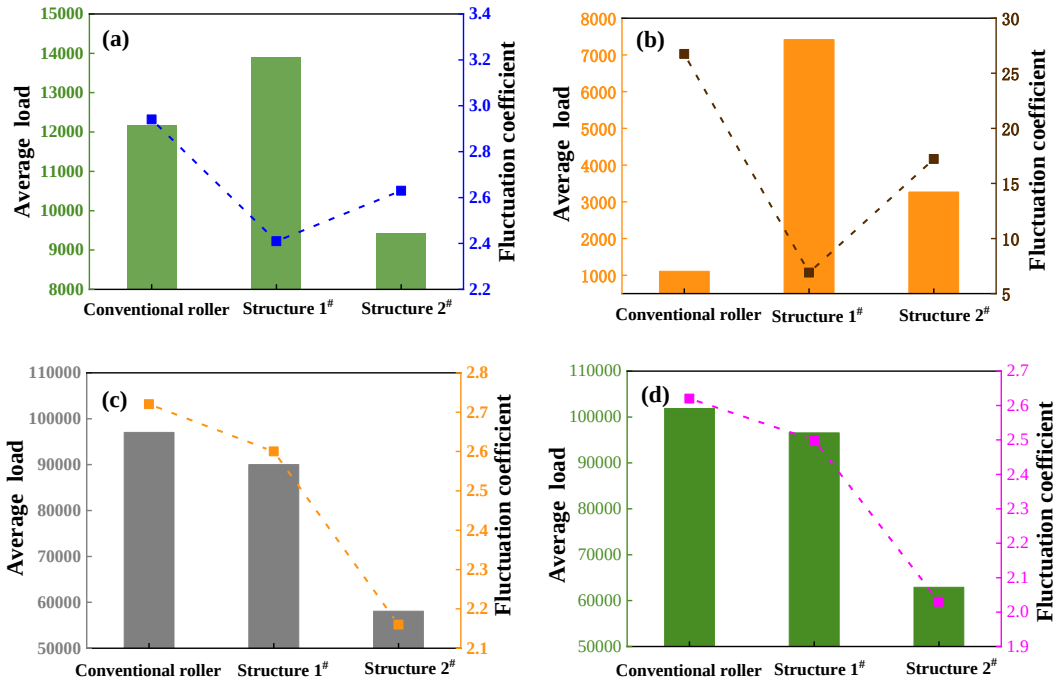

Figure 11. Load Effectiveness of Rollers Before and After Optimization (a) X-axis (b) Y-axis (c) Z-axis (d) Overall Force.

Experimental results show that Structure 1# significantly reduces the Y-directional load fluctuation of the traditional drum, while also decreasing the mean and fluctuation coefficients of the Z-directional and resultant forces, with the fluctuation coefficient of the resultant force reduced by 4.63%. This is because Structure 1# incorporates Circular curved guide plates at the root of the spiral blades, which can buffer the falling coal particles and reduce impact, thus lowering the load fluctuation of the drum and decreasing the risk of multiple coal particle breakages.

In contrast, Structure 2# reduces the mean and fluctuation coefficients of the X, Y, Z-directional, and resultant forces of the traditional drum, with the fluctuation coefficient of the resultant force reduced by 22.59%. However, Structure 2# exhibits increased mean and fluctuation coefficients in the Y-directional load compared to Structure 1#, as the addition of triangular coal guiding plates in Structure 2# causes some coal particles to change direction at the plates, leading to additional fluctuations and consequently increasing the mean and fluctuation coefficients of the Y-directional load.

In summary, both optimized Structure 1# and Structure 2# significantly improve the coal-loading efficiency of the coal mining machine and reduce the load fluctuation of the drum. While Structure 2# shows a lesser improvement in coal-loading efficiency compared to Structure 1#, its reduction in load fluctuation is more pronounced.

3.3. Co-optimization of Drum Motion Parameters

The optimization of the helical vane structure significantly improved the drum's coal particle coal-loading performance. However, the drum's coal-loading performance is a complex issue with multiple interrelated objectives. To further enhance its performance, it is necessary to perform a collaborative optimization of the drum's structure and motion parameters. This collaborative optimization method can comprehensively consider multiple related objectives, enhancing the overall performance of the drum.

3.3.1. Establishment of the Objective Function

In this section, motion parameters are optimized for structure 2# with better coal-loading performance. Selecting traction speed v_q and rotation speed n as design variables:

$$X = [v_q, n] \tag{10}$$

Establishing a multi-objective optimization function for the helical drum aims to maximize the coal-loading efficiency η, minimize the load fluctuation δ, and minimize the loading power H_w. In order to adapt to different working conditions,

three rotational speeds of 43.3, 50.4 and 58.9 r/min and three traction speeds of 50, 110 and 180 mm/s were selected to conduct simulation tests on the coal-loading efficiency, load fluctuation and loading power of Structure 2#, and the relationship between the design variables and optimization objectives was established, as shown in Figure 12 below.

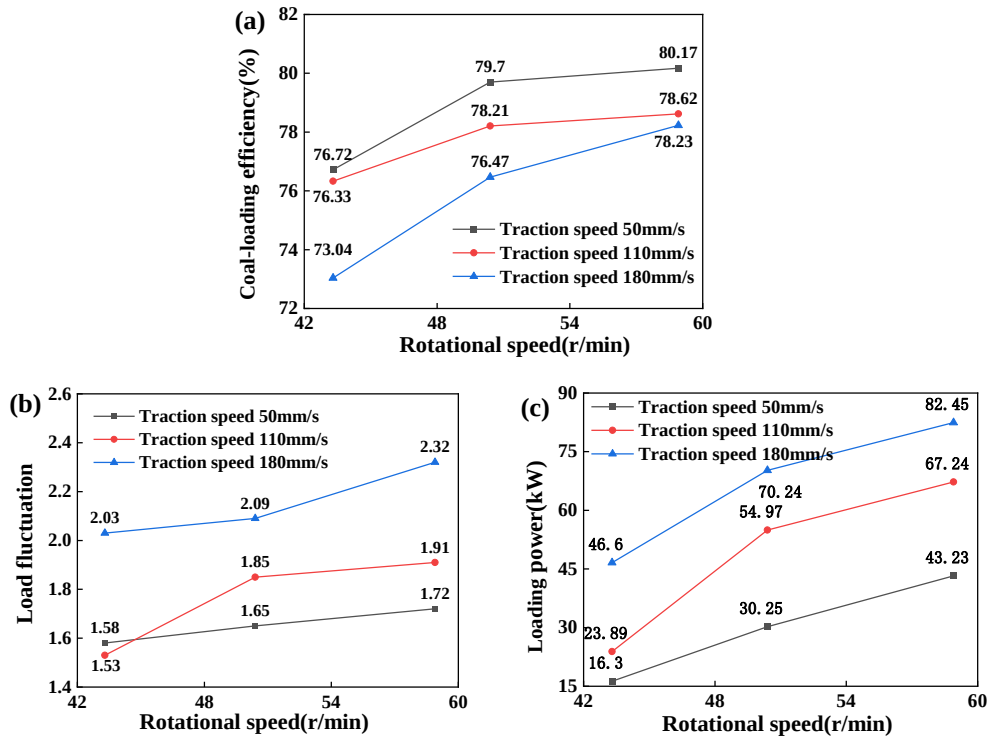

Figure 12. Relationship Diagram between Design Variables and Optimization Objectives (a) Relationship between Coal-loading Efficiency and Traction Speed and Speed (b) Relationship between Load Fluctuation and Traction Speed and Speed (c) Relationship between Loading Power and Traction Speed and Speed.

As shown in Figure 12(a), the high-speed rotation of the drum applies greater centrifugal force to the coal particles, increasing their movement speed and facilitating their discharge towards the coal discharge port. Simultaneously, high-speed rotation reduces the contact time between the coal particles and the drum of the shearer, intensifying the force exerted on the coal particles, enhancing their crushing ability, and thus improving the coal-loading efficiency. Consequently, the coal-loading efficiency of the shearer increases with the increase in rotational speed.

When the rotational speed increases from 43.3 r/min to 50.4 r/min, the coal-loading efficiency increases by an average of 3.68%. Further, from 50.4 r/min to 58.9 r/min, the coal-loading efficiency increases by an average of 1.14%. However, as the rotational speed continues to increase, the rapid increase in the number of coal particles in the drum leads to congestion at the coal discharge port, slowing down the rate of improvement in coal-loading efficiency. Additionally, the coal-loading efficiency decreases with the increase in traction speed, consistent with the previously observed trend.

As illustrated in Figure 12(b), under high-speed cutting conditions, the shearer's drum generates greater impact force, reducing its stability. The coal is crushed into smaller volumes, causing larger fluctuations in load. Consequently, load fluctuations increase with increasing rotational and traction speeds.

As depicted in Figure 12(c), increasing the traction speed results in greater friction and resistance to the movement of coal particles on the drum, requiring more power to overcome these resistances. With the increase in drum rotational speed, the power required for cutting coal walls also increases. Hence, the loading power of the drum increases with the increase in rotational and traction speeds.

Based on the experimental results, fitting the data of the objective quantity and design variables yields the objective function, as shown in Equation (11).

$$\begin{cases} \eta = -0.0001835n^2 - 0.0000004973{v_q}^2 + 0.000009197v_q n - 0.0005809v_q + 0.02005n + 0.2587 \\ \delta = -0.0004493n^2 + 0.00002759{v_q}^2 + 0.00007222v_q n - 0.0062v_q + 0.05504n + 0.08838 \\ H_w = -0.1125n^2 - 0.0004585{v_q}^2 + 0.003932v_q n + 0.1863v_q + 13.32n - 370.2 \end{cases} \quad (11)$$

Before optimization, the range of design variables is constrained. The traction speed was set between 50 and 180 mm/s, while the rotational speed was set between 40 and 60 r/min.

3.3.2. Multi-objective Optimization Algorithm Selection and Crowding Calculation Defects

The Non-Dominated Sorting Genetic Algorithm II (NSGA-II) is one of the most mainstream multi-objective optimization algorithms. Its primary advantage is the use of non-dominated sorting to rank individuals in the population, assigning each individual a specific rank. Within the same rank, individuals are sorted in ascending order based on their objective values, and the distance between adjacent individuals is calculated as the crowding distance value, with the sum of all crowding distance values across objectives calculated as the total crowding distance. For two sub-objectives f_1 and f_2, the crowding distance of an individual i is the sum of the lengths and widths of the dashed rectangles, as shown in Figure 13. Thus, the total crowding distance of individual i is calculated as follows.

$$D_{ij} = D_{ij} + \frac{f_{(i+1)j} - f_{(i-1)j}}{f_{\max j} - f_{\min j}} \quad (12)$$

In the equation, j represents the sub-objective index, $j = 1,2$;

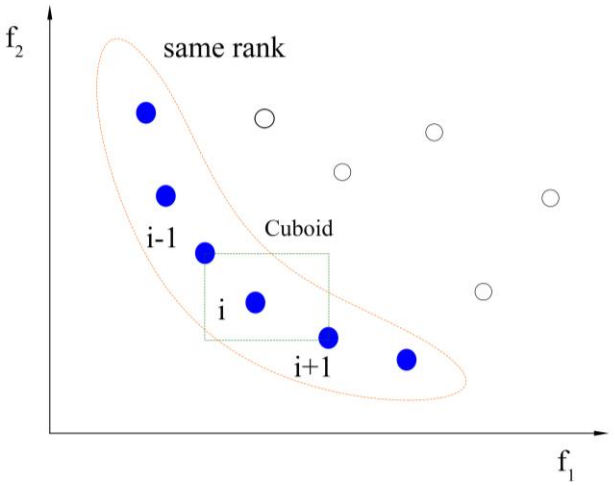

Figure 13. Crowding Illustration.

The crowding distance calculation method has some drawbacks when dealing with three or more objectives, leading to inaccurate crowding distance calculation for certain individuals. Taking three objectives as an example for illustration, as shown in Figure 14.

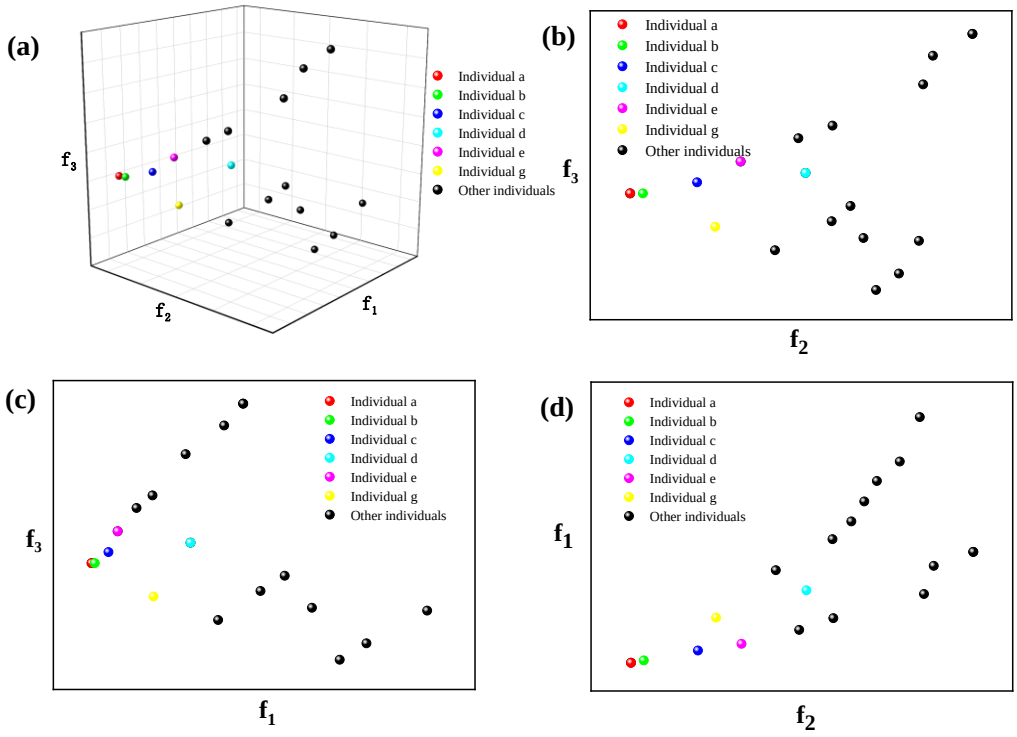

Figure 14: Distribution Chart of Individuals with the Same Rank for Three Objectives(a)Isometric side diagram(b)Left view (c)Right view and (d)Top view

In the above figure, individuals a, b, c, and d are located in the same rank, and they are close to each other, so it is not suitable to use them as parents for further iterations. According to the NSGA-II method, when calculating the total crowding distance value of individual c, the fitness values of each individual on each objective are sorted. On objective f_3, the neighboring individuals of individual c are individuals b and d; on objective f_2, the neighboring individuals of individual c are individuals b and g; on objective f_1, the neighboring individuals of individual c are individuals b and e. The accuracy of the total crowding is affected by the fact that individuals need to be reordered at each goal, resulting in individuals c having different neighboring individuals after a single goal ordering.

3.3.3. NSGA-II Algorithm Improvement Strategy

The analysis above shows that the NSGA-II algorithm, when calculating three or more objectives, tends to confuse neighboring individuals during the computation of crowding distance. This leads to inaccurate total crowding distance calculations, resulting in uneven population distribution and poor diversity of the Pareto front in the iterative process. To address these issues, this paper proposes an improved strategy for the NSGA-II algorithm based on spatial density, termed SD-NSGA-II. This strategy mainly improves the crowding distance calculation method of the NSGA-II algorithm by defining the crowding distance through the number of individuals surrounding each individual. This avoids misidentification between individuals and more accurately calculates the degree of crowding between individuals, thereby increasing the uniformity of the population distribution and improving the diversity of the Pareto solution set.

Taking individual c as an example, firstly, fitness of all individuals is calculated and sorted on one of the objectives. Then, a sphere is constructed with individual c as the center and radius R_a, as shown in Figure 15. The number of individuals falling within this sphere is counted, and this count is defined as the spatial density ρ_s of individual c. Next, the spatial density of individuals in the same generation is calculated and sorted in ascending order, with smaller density values given priority for reproduction in the next generation.

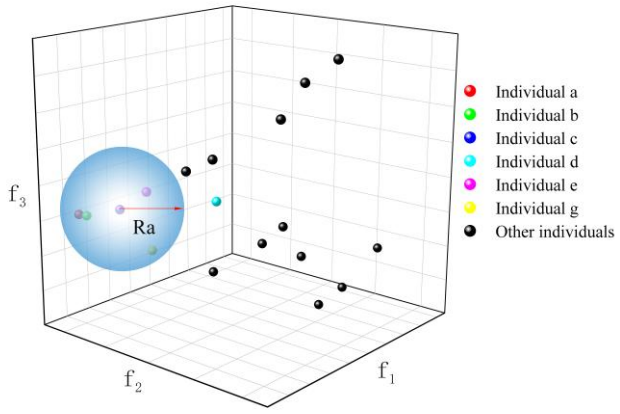

Figure 15. Spatial Density Diagram of Individual 5.

By using spatial density instead of crowding distance calculation, the problem of uneven distribution of individuals caused by multiple sorting can be avoided. This method can more effectively describe the distribution of individuals in the search space, thereby providing more accurate calculations for solving multi-objective optimization problems.

The selection of the spatial radius R_a will affect the accuracy of the spatial density ρ_s. An excessively large spatial radius can result in many identical spatial density values within the population, making it difficult to select superior offspring for reproduction. Conversely, an excessively small spatial radius will cause all individual spatial densities to be 1, making it impossible to distinguish excellent individuals. Therefore, whether the spatial radius is too large or too small will affect the true density values around individuals.

This paper proposes the concept of an adaptive radius, which calculates the sum of the Euclidean distances of all individuals in each generation and determines the average Euclidean distance between individuals. This average distance is then multiplied by the radius coefficient K_r to obtain the adaptive radius R_a for each generation, as shown in Equation (13).

$$R_a = \frac{K_r}{N}\sum_{i=1}^{N}\sqrt{(x_{i+1}-x_i)^2+(y_{i+1}-y_i)^2+(z_{i+1}-z_i)^2} \quad (13)$$

In the equation, K_r represents the radius coefficient, N represents the total number of individuals in the same generation.

3.3.4. Implementation of SD-NSGA-II Algorithm

Based on the improved NSGA-II algorithm, the multi-objective optimization flowchart is shown in Figure 16.

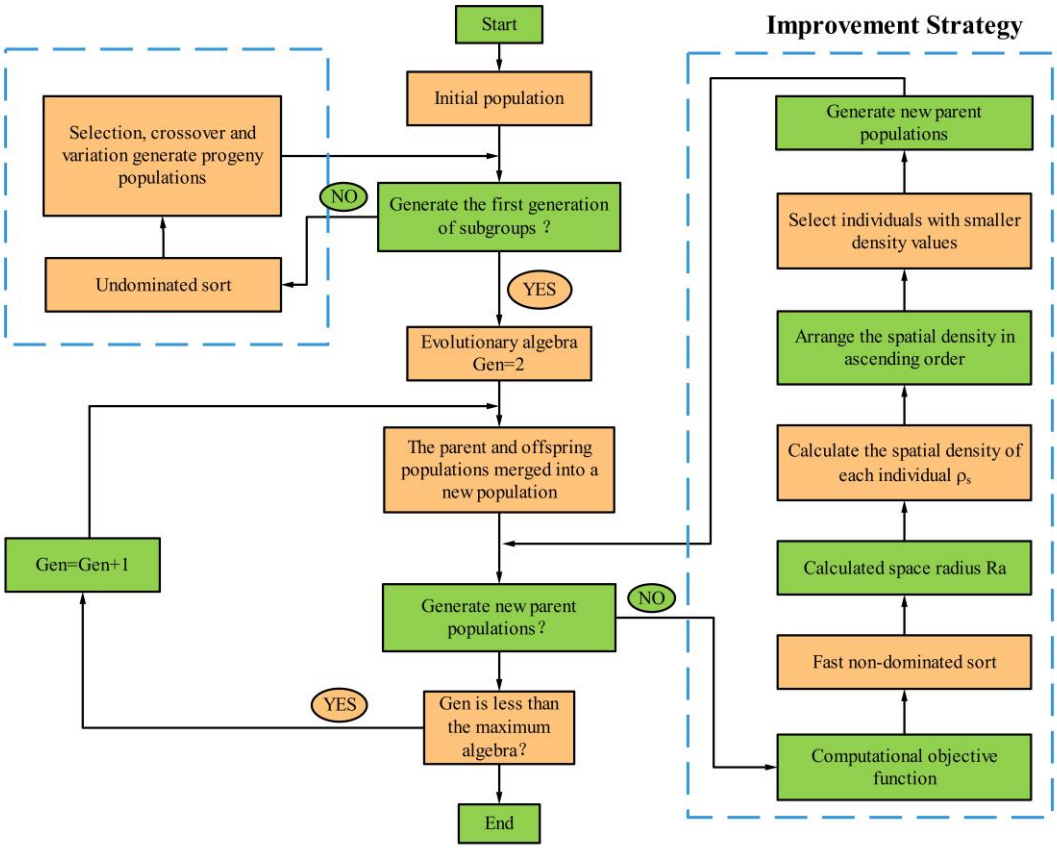

Figure 16. Flowchart of the SD-NSGA-II algorithm.

Step 1: Initialize the population. Randomly initialize individuals according to the constraint conditions, set the population evolution parameters, and set the generation number to Gen=1.

Step 2: Determine if the first generation offspring population has been generated. If so, set the generation number to Gen=2; otherwise, perform non-dominated sorting on the initialized population and generate the first generation offspring population through selection, crossover, and mutation operations, then set the generation number to Gen=2.

Step 3: Combine the parent population and offspring population into a new population.

Step 4: Determine if a new parent population has been generated. If not, calculate the objective function values of individuals in the new population, perform fast non-dominated sorting, calculate the spatial radius R_a of individuals in this generation, then calculate the spatial density ρ_s of individuals, rank the spatial density, and select individuals with smaller spatial density values according to the new population setting to generate the new parent population; otherwise, proceed to Step 5.

Step 5: Perform selection, crossover, and mutation operations on the generated parent population to produce the offspring population.

Step 6: Check if Gen equals the maximum number of generations. If not, set Gen=Gen+1 and return to Step 3; otherwise, end the algorithm and output the Pareto front.

3.3.5. Multi-Objective Optimization Results and Analysis

In this study, the SD-NSGA-II multi-objective algorithm optimization program is implemented in MATLAB software, with a population size set to 100, Pareto solution set size set to 100, and the number of iterations set to 50. And through multiple trials, it was found that the population distribution was optimal when the radius coefficient $K_r=2$.

To compare the effectiveness and practicality of this improved algorithm, the same parameters as the NSGA-II algorithm were selected. After running the program, the Pareto solution set distributions of the two algorithms were obtained, as shown in Figure 17 below.

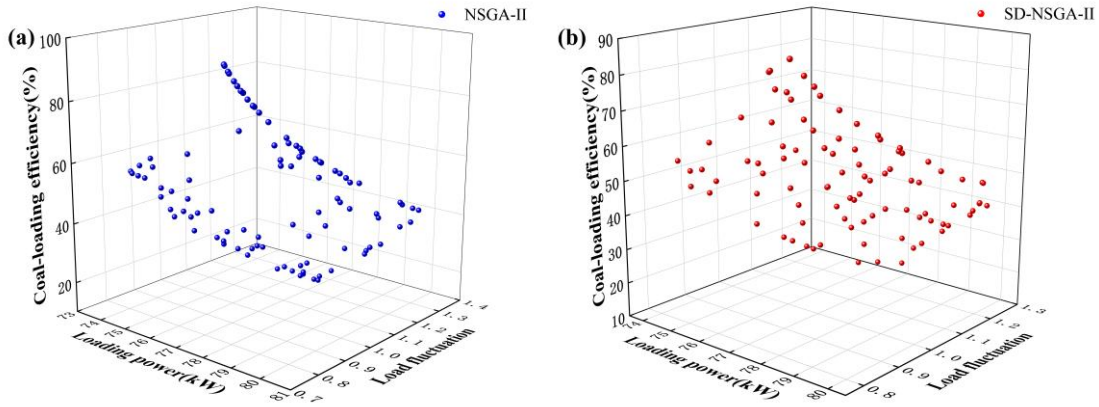

Figure 17. Comparison of Pareto Solution Set Distribution (a) Pareto Solution Set of NSGA-II Algorithm (b) Pareto Solution Set of SD-NSGA-II Algorithm.

Comparing the Pareto solution set distributions of the two algorithms, it can be observed that the distribution of the NSGA-II algorithm's solution set is uneven, with poor population diversity. This leads to high solution density in some regions and sparsity in others, resulting in a lack of optimal solutions in certain areas. In contrast, the spatial distribution of the solution set obtained by the SD-NSGA-II algorithm is more uniform, making the resulting solution set more representative and comprehensive. In practical applications, the solution set obtained by the SD-NSGA-II algorithm is more likely to contain more effective solutions, providing more space for selection and decision-making information, thereby improving the quality of problem-solving and decision-making reliability.

Furthermore, by introducing the concept of adaptive radius, the SD-NSGA-II algorithm can dynamically adjust spatial density based on the distribution of solutions, further improving the algorithm's convergence speed and accuracy. This adaptability gives SD-NSGA-II an advantage in dealing with complex multi-objective optimization problems, enabling it to find a uniform Pareto solution set more quickly.

3.3.6. Selection of Pareto Optimal Solutions

In engineering applications, decision-makers often wish to select a set of optimal solutions from the Pareto solution set for the final decision. To achieve this, this paper adopts the Entropy Weight-TOPSIS method based on subjective judgment to obtain the Pareto optimal solution. This method first utilizes the entropy weight method to determine the weights of evaluation indicators, and then combines subjective weights for adjustment. Subsequently, the TOPSIS method is employed to analyze the new data. This approach comprehensively considers the similarity between the positive ideal solution and the negative ideal solution, thoroughly evaluating the merits of each solution and selecting the solution with the highest score as the optimal one. The following are the specific steps of the Entropy Weight-TOPSIS method based on subjective judgment:

(1) Determine the decision matrix: Based on the Pareto solution set, determine the decision matrix P.

$$P = \begin{bmatrix} p_{11} \cdots p_{a1} \cdots p_{b1} \\ p_{12} \cdots p_{a2} \cdots p_{b2} \\ p_{13} \cdots p_{a3} \cdots p_{b3} \end{bmatrix} \tag{14}$$

In the equation, p_{ac}represents the c^{th}Pareto solution in the a^{th} objective, $c = 1,2,3$; b represents the total number of solutions for each objective.

(2) Data Standardization: Standardize the dimensions and units of the three objectives, namely loading efficiency, load fluctuation, and shipping power, by normalizing the decision matrix, as shown in equation (15).

$$q_{ac} = \begin{cases} \frac{p_{ac} - min\, p_{ac}}{max\, p_{ac} - min\, p_{ac}} & 1 \le a \le b, c = 1,3 \\ \frac{max\, p_{ac} - p_{ac}}{max\, p_{ac} - min\, p_{ac}} & 1 \le a \le b, c = 2 \end{cases} \tag{15}$$

In the equation, q_{ac} represents the a^{th} solution in the c^{th} normalized objective function; $max\, p_{ac}$ represents the maximum Pareto solution in the c^{th} objective function, and $min\, p_{ac}$ represents the minimum Pareto solution in the c^{th}objective function.

(3) Calculate the entropy value$E_c$and weightW_c: for each objective to measure uncertainty and compute weights based on the entropy values.

$$\begin{cases} E_c = -\dfrac{\sum_{a=1}^{b}\left[\frac{q_{ac}}{\sum_{a=1}^{b} q_{ac}} ln\left(\frac{q_{ac}}{\sum_{a=1}^{b} q_{ac}}\right)\right]}{ln\, c} \\ W_{oc} = \dfrac{1-E_c}{\sum_{c=1}^{3}(1-E_c)} \quad c = 1,2,3 \\ W_c = \dfrac{W_{sc}W_{oc}}{\sum_{c=1}^{3} W_{sc}W_{oc}} \end{cases} \tag{16}$$

In the equation, W_{oc} represents the entropy weight, and W_{sc}represents the subjective weight.

(4) Calculate the weighted decision matrix: Multiply the standardized decision matrix by the corresponding weights to obtain the weighted decision matrix.

$$y_{ac} = W_c q_{ac} \quad 1 \le a \le c, c = 1,2,3 \tag{17}$$

(5) Determine the positive ideal solution and negative ideal solution: For each objective function, identify the maximum and minimum values among all solutions to form the positive ideal solution$A^+$and negative ideal solutionA^-respectively.

$$\begin{cases} A_c^+ = max\, y_{ac} \\ A_c^- = min\, y_{ac} \end{cases} \tag{18}$$

(6) Calculate the distance between each solution and the positive ideal solution as well as the negative ideal solution: Use the Euclidean distance to compute the distance between each solution and the positive ideal solution, as well as the negative ideal solution.

$$\begin{cases} D_a^+ = \sqrt{\sum_{c=1}^{3}(y_{ac} - A_c^+)^2} \\ D_a^- = \sqrt{\sum_{c=1}^{3}(y_{ac} - A_c^-)^2} \end{cases} \tag{19}$$

In the equation, D_a^+ represents the distance from the solution$a$to the positive ideal solution, and D_a^-represents the distance from the solution$a$to the negative ideal solution.

(7) Calculate the comprehensive score: Calculate the similarity score for each solution.

$$C_a = \frac{D_a^+}{D_a^+ + D_a^-} \quad 1 \le a \le c \tag{20}$$

The closer the score C_a is to 1, the better the solution a, therefore, the solution with the highest score in the Pareto set is chosen as the compromise optimal solution.

The calculation of Pareto optimal solutions using the subjective judgment-based entropy-weighted TOPSIS method allows decision-makers to determine the importance of solutions according to their preferences and needs, better reflecting the real decision-making environment and requirements. Subjective weights can be chosen based on decision-maker preferences. Taking the subjective weight of $W_{sc} = [0.33,0.33,0.33]$ as an example, the entropy values and weights of the three objectives are calculated based on the Pareto solution set obtained by SD-NSGA-II, as shown in Figure 18 below.

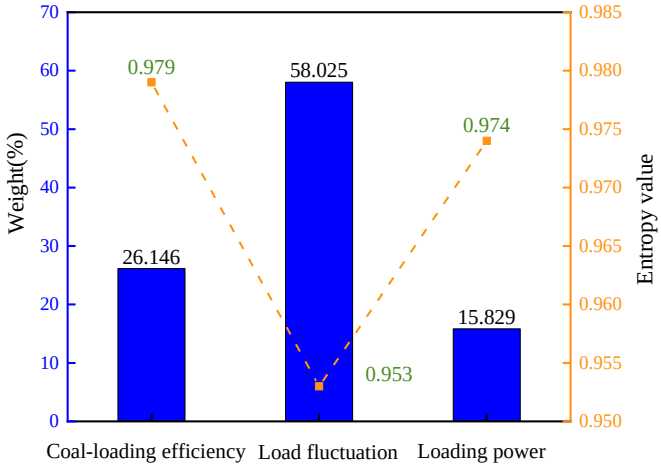

Figure 18. Entropy Values and Weights of Three Objectives.

Based on the weighted calculation, a comprehensive score was obtained, yielding the optimal motion parameters: a traction speed of 135.32 mm/s and a rotation speed of 56.37 r/min. To ensure the effectiveness and reliability of the optimized parameters, a performance comparison was conducted between the optimized drum (Structure 2#) and the traditional drum, as shown in Table 5 below.

Table 5. Comparison of Optimal Solutions Before and After Cooperative Optimization.

	Traction speed (mm·s^{-1})	Rotational speed (r·min^{-1})	Coal-loading efficiency(%)	Load fluctuationδ	Loading power(kW)
Conventional roller	135.32	56.37	72.94	1.64	97.72
Collaborative optimization after roller			78.09	0.88	71.03

Compared to the traditional drum, the synergistically optimized drum achieved significant improvements across all three objectives. The coal-loading efficiency increased by 7.06%, the load fluctuation decreased by 46.34%, and the loading power decreased by 27.31%. Moreover, the combination of the subjective-weighted TOPSIS method with the SD-NSGA-II algorithm not only considered the weight distribution of multiple indicators but also incorporated the

subjective judgments of decision-makers, enhancing the credibility and practicality of the optimization results and providing more reliable optimization solutions for decision-making. In summary, these improvements resulted in a significant enhancement in the coal-loading performance and reliability of the drum, offering valuable references for the design of coal mining machine drums.

4. Conclusion

This paper presents a synergistic optimization design method for drum design and significantly enhances the coal-loading performance of coal mining machines based on the improved NSGA-II algorithm. The main conclusions are as follows:

(1) According to the analysis of coal block movement, it was found that the coal block's speed is positively correlated with rotation speed and helical angle. By optimizing the helical angle of the dual-section differential rotation drum, Gao found that the best coal-loading performance of the drum was achieved at a helix angle of 18° for the front drum and 30° for the rear drum [11]. This study's findings are consistent with this, through simulation experiments under different helical angles and traction speeds, it was found that the coal-loading efficiency of the drum was highest when the helical angle was 18°. However, when the helical angle increased from 18° to 30°, both the axial speed and mass flow rate of the coal flow decreased, leading to reduced coal-loading efficiency. This further validates that coal-loading performance is best at a spiral lift angle of 18°.

(2) Based on the optimal helical angle, this paper designs two types of coal-guiding drums with a helical angle of 18°, adding arc-shaped and triangular coal-guiding plates. The arc-shaped coal guide plate increased the axial speed by altering the coal particle trajectory, while the triangular coal guide plate reduced the generation of floating coal by adjusting the direction of the coal flow on the inner side of the vane. Simulation experiments showed that the coal-loading efficiency of the optimized helical vane drum increased by 9.94%, and load fluctuations decreased by 22.59%. Compared to Sun's modifications of the vane inclination angle [5], this paper achieves a more significant lifting effect by changing the vane shape, which significantly improves the coal-loading efficiency of the coal miner and reduces the load fluctuation of the drum from the perspective of structural optimization.

(3) In order to further improve the performance of the drum, an improvement strategy based on the NSGA-II algorithm is proposed, aiming at optimizing the motion parameters of the coal-guided drum, and the improved algorithm has obvious advantages in terms of the diversity of spatial distributions and solutions of the solution set. The concept of spatial density and adaptive radius is introduced, and the optimal solution is obtained through the subjective-weighted TOPSIS method. The optimal traction speed is determined to be 135.32 mm/s, and the rotation speed is 56.37 r/min. Compared with the traditional drum, the coal-loading efficiency of the synergistically optimized drum increased by 7.06%, the load fluctuation decreased by 46.34%, and the loading power decreased by 27.31%.

Acknowledgements

This work was supported by Project of Shanxi Provincial Science and Technology Major Special Plan (grant number :202201100401016)

References

1. Wang Z, Liu C, Wu J, Jiang H, Zhao Y. Impact of screening coals on screen surface and multi-index optimization for coal cleaning production. Journal of Cleaner Production. 2018;187:562-75. https://doi.org/10.1016/j.jclepro.2018.03.238
2. Yan S, Xu G, Fan Z. Development course and prospect of the 50 years'comprehensive mechanized coal mining in China. Coal Science and Technology. 2021;49(11):1-9.
3. Zhai Y, Shi C, Lv X, Guo D. Development status and key technologies of thin coal seam drum shearer. Coal Engineering. 2020;52(7):182-6.
4. Gao Kd, Xu Wb, Jiang Sb, Du Cl. Factors affecting thin coal seam shearer drum coal-loading performance by a model test method. Journal of Central South University. 2019;26(6):1619-36. https://doi.org/10.1007/s11771-019-4117-4
5. Sun L, Zhang X, Zeng Q, Gao K, Jiang K, Zhou J. Application of a screw conveyor with axial tilt blades on a shearer drum and investigation

of conveying performance based on DEM. Particuology. 2022;61:91-102. https://doi.org/10.1016/j.partic.2021.06.001

6. Zhang X, Gao K, Zeng Q, Lin L, Wu T, Sun L. Numerical Investigation of Effect of Drum Barrel on Coal-Loading Performance of Thin-Coal-Seam Shearer Machines. Machines. 2022;10(4):253. https://doi.org/10.3390/machines10040253
7. Xue J, Gao Y, Huang L, He T. Study on drum load of shearer. Metalurgija. 2023;62(3-4):427-9.
8. Wan L, Jiang K, Zeng Q, Gao K. Dynamic response and reliability analysis of shearer drum cutting performance in coal mining process. Eksploatacja i Niezawodność – Maintenance and Reliability. 2022;24(1):123-9. https://doi.org/10.17531/ein.2022.1.14
9. Meng Z, Ma C, Xie Y. Influence of impact load form on dynamic response of chock-shield support. Eksploatacja i Niezawodność – Maintenance and Reliability. 2023;25(3). https://doi.org/10.17531/ein/168316
10. .Zhang Q, Wang C, Tian Y. Study on shearer drum structure design and coal-breaking performance based on multi-impact picks for hard coal. Environmental Earth Sciences. 2022;81(7):189. https://doi.org/10.1007/s12665-022-10313-z
11. Gao K, Zhang X, Sun L, Zeng Q, Liu Z. Loading performance of a novel shearer drum applied to thin coal seams. Energies. 2021;14(2):358. https://doi.org/10.3390/en14020358
12. Cundall PA. The measurement and analysis of accelerations in rock slopes. Ph D Thesis, Imperial College. 1971.
13. Liu X, Du C, Fu X, Zhao H, Zhang J, Yang X. Wear analysis and performance optimization of drum blade in mining coal gangue with shearer. Engineering Failure Analysis. 2021;128:105542.
14. Liu Y, Wang S, Li K, Sun W, Song X. An Adaptive Two-Stage Kriging-Based Infilling Strategy for Efficient Multi-Objective Global Optimization. Journal of Mechanical Design. 2022;144(11):111706. https://doi.org/10.1115/1.4055122
15. Wu D, Sotnikov D, Gary Wang G, Coatanea E, Lyly M, Salmi T. A Dimension Selection-Based Constrained Multi-Objective Optimization Algorithm Using a Combination of Artificial Intelligence Methods. Journal of Mechanical Design. 2023;145(8). https://doi.org/10.1115/1.4062548
16. Zhou B, Li S, Zi B, Chen B, Zhu W. Multi-objective optimal design of a cable-driven parallel robot based on an adaptive adjustment inertia weight particle swarm optimization algorithm. Journal of Mechanical Design. 2023;145(8). https://doi.org/10.1115/1.4062458
17. Ma H, Zhang Y, Sun S, Liu T, Shan Y. A comprehensive survey on NSGA-II for multi-objective optimization and applications. Artificial Intelligence Review. 2023;56(12):15217-70. https://doi.org/10.1007/s10462-023-10526-z
18. Jiang R, Ci S, Liu D, Cheng X, Pan Z. A hybrid multi-objective optimization method based on NSGA-II algorithm and entropy weighted TOPSIS for lightweight design of dump truck carriage. Machines. 2021;9(8):156. https://doi.org/10.3390/machines9080156
19. Li X, Qu H, Li G, Guo S, Dong G. Optimal Design of a Kinematically Redundant Planar Parallel Mechanism Based on Error Sensitivity and Workspace. Journal of Mechanical Design. 2023;145(2):023305. https://doi.org/10.1115/1.4056202
20. Wang Y, Liao X, Lu J, Ma J. Optimization Method of Sheet Metal Laser Cutting Process Parameters under Heat Influence. Machines. 2024;12(3):206. https://doi.org/10.3390/machines12030206
21. Yuan M, Li Y, Zhang L, Pei F. Research on intelligent workshop resource scheduling method based on improved NSGA-II algorithm. Robotics and Computer-Integrated Manufacturing. 2021;71:102141.
22. Zhi P, Wang Z, Tian Z, Lu J, Wu J, Guo X, et al. Fracture mechanism analysis and design optimization of a wheelset lifting mechanism based on experiments and simulations. Machines. 2022;10(5):397. https://doi.org/10.3390/machines10050397
23. Foroughi S, Hamidi JK, Monjezi M, Nehring M. The integrated optimization of underground stope layout designing and production scheduling incorporating a non-dominated sorting genetic algorithm (NSGA-II). Resources Policy. 2019;63:101408.
24. Li Y-H, Sheng Z, Zhi P, Li D. Multi-objective optimization design of anti-rolling torsion bar based on modified NSGA-III algorithm. International Journal of Structural Integrity. 2021;12(1):17-30. https://doi.org/10.1108/IJSI-03-2019-0018
25. Zhang P, Qian Y, Qian Q. Multi-objective optimization for materials design with improved NSGA-II. Materials Today Communications. 2021;28:102709.
26. Wei H, Liang J, Li C, Zhang Y. Real-time locally optimal schedule for electric vehicle load via diversity-maximization NSGA-II. Journal of Modern Power Systems and Clean Energy. 2020;9(4):940-50. https://doi.org/10.35833/MPCE.2020.000093
27. Liu X, Li X, Fu X, Yang X, Zhang J. Analysis on the influence law of traction speed on the cutting performance of coal containing hard concretion. Mechanics & Industry. 2023;24:5. https://doi.org/10.1051/meca/2023001
28. Hao J, Yang X, Wang C, Tu R, Zhang T. An improved NSGA-II algorithm based on adaptive weighting and searching strategy. Applied

Sciences. 2022;12(22):11573. https://doi.org/10.3390/app122211573

29. Chen S, Zhang X, Li Q, Shen C, Shi Y. The vertical screw conveying characteristics of cohesive particle and optimization of design parameters. Eksploatacja i Niezawodność – Maintenance and Reliability. 2023;25(1). https://doi.org/10.17531/ein.2023.1.13
30. Zhao H, Zhang C. Multi parameter optimization design of shearer drum based on LS-DYNA. Manufacturing Automation. 2023;45(03):144-7.
31. Wang J. Numerical Simulation Study on Optimization of Coal Miner Cut-Off. Mechanical Management and Development. 2023;38(08):124-5.
32. Liu S, Li H, Jiang H, Zhang Q, Cui Y, Liu X. Research progress and prospect of coal-rock breaking methods in mines. Journal of China Coal Society. 2023;48(02):1047-69.
33. Yao Y. Study on influence of shearer drum parameters on loading efficiency. Mining Equipment. 2023(12):185-7.
34. Zhao L, Wang Y, Wang B. Analysis and Prediction of Working Performance of Shearer Spiral Drums under Coal Seam with Gangue. China Mechanical Engineering. 2021;32(08):976-86.
35. Song S, Luo J, Wan F, Li B. Influence of Hydra cutter tooth installation angle on cutting load. Journal of Heilongjiang University of Science and Technology. 2020;30(05):511-8.
36. Zhou Y. Research and Simulation Analysis on the Cut-off Performance of Mine Roller Coal Mining Machine. Mechanical Management and Development. 2023;38(04):7-8+11.
37. Zhang Q, Zhang X. Wear characteristics of shearer pick. Journal of Liaoning Technical University(Natural Science). 2021;40(05):430-9.
38. Tian Z. Working Characteristic Research of Thin Seam Shearer Drum [PHD thesis]2016.